Nanoscale

Synthesis of luminescent core/shell α-Zn_3P_2/ZnS quantum dots

Journal:	*Nanoscale*
Manuscript ID	NR-ART-09-2020-006665
Article Type:	Paper
Date Submitted by the Author:	16-Sep-2020

Complete List of Authors:	Paredes, Ingrid; New York University, Chemical and Biomolecular Engineering Beck, Clara; Federal Institute of Technology (ETHZ), Engineering Lee, Scott; New York University, Chemical and Biomolecular Engineering Chen, Shuzhen; New York University, Chemical and Biomolecular Engineering Khwaja, Mersal; New York University, Chemical and Biomolecular Engineering Scimeca, Michael; New York University, Chemical and Biomolecular Engineering Li, Shuang; Brookhaven National Laboratory Hwang, Sooyeon; Brookhaven National Laboratory, Center for Functional Nanomaterials Lian, Zhen; Rensselaer Polytechnic Institute, Chemical and Biological Engineering McPeak, Kevin; Louisiana State University College of Agriculture, Chemical Engineering Shi, S; Rensselaer Polytechnic Institute, Chemical and Biological Engineering Sahu, Ayaskanta; New York University, Chemical and Biomolecular Engineering

Synthesis of luminescent core/shell α-Zn_3P_2/ZnS quantum dots

*Ingrid J. Paredes, Clara Beck, Scott Lee, Shuzhen Chen, Mersal Khwaja, Michael R. Scimeca, Shuang Li, Sooyeon Hwang, Zhen Lian, Kevin M. McPeak, Su-Fei Shi, Ayaskanta Sahu**

Department of Chemical and Biomolecular Engineering, New York University, Brooklyn, NY 11201

E-mail: asahu@nyu.edu

Clara Beck

Optical Materials Engineering Laboratory, ETH Zurich, 8092 Zurich, Switzerland

Shuang Li, Sooyeon Hwang

Center for Functional Nanomaterials, Brookhaven National Laboratory, Upton, NY 11973

Zhen Lian, Prof. Su-Fei Shi

Department of Chemical and Biological Engineering, Rensselaer Polytechnic Institute, Troy, NY 12180

Prof. Kevin M. McPeak

Department of Chemical Engineering, Louisiana State University, Baton Rouge, LA, 70803

Keywords: metal phosphides, zinc phosphide, quantum dots, core shell, colloidal synthesis

Abstract:

Metal chalcogenide nanoparticles offer vast control over their optoelectronic properties via size, shape, composition, and morphology which has led to their use across fields including optoelectronics, energy storage, and catalysis. While cadmium and lead-based nanocrystals are prevalent in applications, concerns over their toxicity have motivated researchers to explore alternate classes of nanomaterials based on environmentally benign metals such as zinc and tin. The goal of this research is to identify material systems that offer comparable performance to existing metal chalcogenide systems from abundant, recyclable, and environmentally benign materials. With band gaps that span the visible through the infrared, II–V direct band gap semiconductors such as tetragonal zinc phosphide (α-Zn_3P_2) are promising candidates for use in optoelectronics. To date, syntheses of α-Zn_3P_2 nanoparticles have been hindered because of the toxicity of zinc and phosphorus precursors, surface oxidation, and defect states leading to carrier trapping and low photoluminescence quantum yield. This work reports a colloidal synthesis of quantum confined α-Zn_3P_2 nanoparticles from common phosphorus precursor tris(trimethylsilyl)phosphine and environmentally benign zinc carboxylates. Shelling of the nanoparticles with zinc sulfide is shown as a method of preventing oxidation and improving the optical properties of the nanoparticles. These results show a route to stabilizing α-Zn_3P_2 nanoparticles for optoelectronic device applications.

1. Introduction

The control that metal chalcogenide nanoparticles offer over their optical and electronic properties via size, shape, and structure tunability has led to their use across fields including optoelectronics, energy storage, and catalysis. While cadmium and lead-based chalcogenides are the most prevalent in applications, concerns over the toxicity of both elements have motivated researchers to explore different classes of nanomaterials.[1-3] Recently, a core/shell system of InP/ZnSe/ZnS quantum dots achieved quantum efficiency of nearly 100%.[4] Concerns over the price of indium, however, have already caused

concern over its widescale deployment in optoelectronics.[5] Similarly, since their introduction in 2009, perovskite-based devices have received significant attention; after a decade of research, a perovskite-based device achieved a power conversion efficiency of 23.7%.[6] Still, researchers must address issues including the stability of perovskites and toxicity of lead to achieve widespread implementation of perovskites.[6] Copper zinc tin sulfide (CZTS) materials offer a sustainable alternative and have already been explored for photovoltaics; to date, devices based on CZTS materials have achieved efficiencies of up to 13%.[7] Literature reports that efficiencies have been hindered by disorder of copper and zinc cations within the crystal structure with no effective solution in sight.[8] This motivates the further search for a new class of materials with a potential for a tunable band gap made from abundant, recyclable, and environmentally benign materials.

The II–V direct band gap semiconductors have been identified as potential candidates for use in optoelectronics; their band gaps span the visible through the infrared, and they have the ability to form alloys of all compositions.[9] Of the II-V semiconductors, tetragonal zinc phosphide (α-Zn_3P_2) has long garnered research interest, particularly for its potential as a photovoltaic material.[9-26] The compound has an ideal band gap (1.5 eV), large absorption coefficient (>10^5 cm^{-1}), and long minority carrier diffusion length (5-10 μm).[16, 20, 27] Further study of Zn_3P_2 has been slow, however, in part because existing routes to bulk, phase-pure, stoichiometric zinc phosphide are energy intensive, expensive and difficult to scale.[21, 24, 28-30] Recent research has explored routes to α-Zn_3P_2 nanostructures including nanoparticles,[31-43] nanowires,[44-56] nanobelts,[57-58] and nanotrumpets,[59] as they present the potential for low production costs and reduced post-synthetic processing costs. Colloidal synthesis routes also offer the potential to easily tune the optoelectronic properties of α-Zn_3P_2 via quantum confinement.[35] Only a few groups, however, have reported implementation of α-Zn_3P_2 nanoparticles in devices.[38, 41] Typically, synthesized nanoparticles have displayed poor crystallinity and low PL quantum yield (at most 2%), thus limiting their applicability in optoelectronic devices.[32, 35-37, 41-42, 60-61] Issues have been attributed to the poor

reactivity of zinc precursors, [2] susceptibility of zinc phosphide to oxidation, [62] and poor charge transport due to the presence of impurities. [38-39]

Efforts to address these issues have had mixed results. In one case, presence of ZnO at the surface has actually improved photoluminescence; however, the phase and stoichiometry of the nanoparticles could not be confirmed. [41] Use of incredibly reactive tris(trimethylsilyl)phosphine ($P(SiMe_3)_3$) with various zinc precursors can provide highly crystalline α-Zn_3P_2, but the optoelectronic properties of these nanoparticles have varied based on synthetic conditions. Most routes that require $P(SiMe_3)_3$ have also required the use of alkyl zinc compounds, such that the synthetic conditions are overall dangerous, pyrophoric, toxic, and expensive. [32-33, 35, 37-39, 41] Such routes to zinc phosphide are therefore unviable routes for sustainable development of Zn_3P_2 devices.

In this work, we report the colloidal synthesis of zinc phosphide nanoparticles from benign zinc carboxylates – zinc acetate and zinc oleate – in place of alkyl zinc compounds. Note that $P(SiMe_3)_3$ is still pyrophoric and should be handled with care. Our goal is to first search for a viable and safer zinc precursor followed by a suitable phosphorus precursor in the future. Previous attempts to use zinc carboxylates have resulted in particles of ambiguous crystallinity; only combining zinc carboxylates with alkyl zincs or $P(SiMe_3)_3$ improved their reactivity.[32, 41, 43] In our synthesis, however, we generated crystalline zinc phosphide nanocrystals by complexing zinc carboxylates with a mixture of benign coordinating ligands trioctylphosphine oxide, trioctylphosphine, and octadecylamine.[63] To our knowledge, this is the first report of crystalline Zn_3P_2 and core/shell Zn_3P_2/ZnS nanoparticles from this route. We studied the effect of injection time, temperature, and concentration of zinc and phosphorus precursors on nanocrystal growth. We tuned the size of the nanoparticles by varying injection temperature and growth time, though no changes in optical properties were observed. The absorbance spectra of the nanoparticles exhibited no excitonic features, and the particles, regardless of their size, showed no detectable photoluminescence at room temperature. We present shelling of the nanoparticles with zinc

sulfide as a method of preventing oxidation and improving photoluminescence quantum yields. Zinc sulfide (ZnS), a semiconductor with a wide band gap of 3.7 eV, has been used to shell several II-VI and III-V semiconductor nanoparticles.[64] Previously, Zn_3P_2/ZnS heterojunctions, heterostructures, and core/shell nanowires have been reported, but to our knowledge, we report the first synthesis of Zn_3P_2/ZnS nanoparticles.[44, 50, 65-66] We present two methods of shelling that result in peak luminescence at 520 nm. These results show a route to more stable α-Zn_3P_2 nanoparticles for further optoelectronic study.

2. Experimental Section

2.1. Chemicals

Octadecylamine (90%, technical), trioctylphosphine oxide (90%, technical), zinc acetate dihydrate (99.999% trace metal basis), thioacetamide (99.0%, ACS reagent), oleic acid (90%, technical), 1-octadecene (90%, technical), N,N-dimethylformamide (99.8%, anhydrous), ethanol (200 proof, anhydrous, ≥ 99.5%), hexane (anhydrous, 95%), methanol (99.8%, anhydrous), trioctylphosphine (90%, technical), and tris(trimethylsilyl)phosphine ($P(SiMe_3)_3$) (95%) were purchased from Sigma Aldrich. Acetone (99.8%, extra dry) and sulfur powder (≥ 99.5%, powder, precipitated) were purchased from VWR. All chemicals were used as purchased without any further purification.

2.1.1. Preparation of zinc oleate.

Zinc oleate was prepared using a method by Boercker *et al*.[67] Zinc acetate dihydrate (1.1 g, 5 mmol) and oleic acid (8 ml) were mixed under vacuum at 110 °C for 2 hours. The solution was then cooled under air and left overnight to produce a sticky, white solid. The solid was then precipitated three times to remove excess oleic acid using acetone via centrifugation at 5000 rpm for 5 minutes. Excess acetone was then removed by placing the solid under vacuum at room temperature. We obtained a white powder that was stored in air for future use.

2.2. Synthesis of Zn_3P_2 nanoparticles

Zinc acetate or zinc oleate (0.81 mmol), trioctylphosphine oxide, (1 g, 2.6 mmol), and octadecylamine (3 g, 11.0 mmol) were mixed in 15 to 60 ml of 1-octadecene in a 100 ml three-neck flask at 1000 rpm. The temperature of the mixture was increased to 70°C. At 30°C, trioctylphosphine (4 ml), shown to slow the consumption of $P(SiMe_3)_3$,[39] was injected into the reaction mixture, producing a colorless solution. At 70°C, the solution was degassed for approximately one hour by alternating the reaction atmosphere between vacuum and nitrogen. The temperature was then raised to 220°C under nitrogen to prepare the mixture for injection. At temperatures between 160°C to 220°C, $P(SiMe_3)_3$ (0.16 ml) diluted in degassed 1-octadecene (2 ml) was swiftly injected into the mixture. The temperature was then set to 220°C for growth for 1 to 4 hours. Upon injection, the reaction mixture darkened gradually from clear yellow to dark red within one minute.

After growth, the solution was cooled slowly to room temperature and transferred into the glovebox for extraction and cleaning of the nanoparticles. Inside the glovebox, the mixture was divided evenly between two 50 ml centrifuge tubes. Methanol (20 ml) was added to each tube, prompting phase separation between methanol and 1-octadecene. The top layer, containing methanol and unreacted material, was removed using a glass pipette. This procedure was repeated until the top layer appeared clear and colorless, indicating that most of the unreacted material in the flask had been removed. Then, acetone (20 ml) was added to each tube to wash remaining 1-octadecene from the nanoparticles. The mixtures were then centrifuged at 9500 rpm for 5 minutes to precipitate out the nanoparticles, a red-brown powder. The supernatant was tossed. Hexanes (5 ml) and acetone (20 ml) were then added to each tube in order to crash out the particles; the hexanes was added in order to improve the dispersibility of the nanoparticles in solution. The mixtures were centrifuged at 9500 rpm for 5 minutes, and the supernatant was removed. The particles were finally dried under vacuum and stored as a dry powder in a nitrogen filled glovebox.

2.3. Shelling of Zn_3P_2 nanoparticles using ZnS

The amount of Zn and S precursors were calculated under the assumption that a single monolayer of ZnS would be added in each reaction. Details of calculations and preparation of zinc and sulfur precursors can be found in the Supporting Information.

2.3.1. Method 1: Using zinc acetate and sulfur powder.

Preparation of zinc precursor for the ZnS shell.

A 0.02 M solution of zinc was prepared by mixing zinc acetate (148 mg, 0.81 mmol), trioctylphosphine oxide (1 g, 2.6 mmol), and octadecylamine (3 g, 11 mmol) in 1-octadecene (30 ml, 93.7 mmol) in a 100 ml three-neck flask at 1000 rpm. The temperature of the mixture was increased to 70°C to produce a clear, colorless solution. At 70°C, the solution was degassed for approximately one hour by alternating the reaction atmosphere between vacuum and nitrogen. The mixture was then cooled to 50°C for injection.

Preparation of sulfur precursor.

A 0.04 M solution of sulfur in 1-octadecene was prepared in a 100 ml three-neck flask by dissolution of sulfur powder. The reaction mixture was degassed at 70°C and then cooled to room temperature for injection.

Synthesis of core/shell Zn_3P_2/ZnS nanoparticles.

Clean core Zn_3P_2 nanoparticles (60 mg) and octadecylamine (3 g, 11 mmol) were dispersed in hexanes (10 ml) and degassed 1-octadecene (5 ml) in a 250 ml three-neck flask. The temperature was raised to 160°C, with a stopper punctured with a needle to relieve pressure buildup within the flask as hexanes evaporated. After hexanes evaporated, the temperature was raised to 220°C. At this temperature, sulfur precursor was injected dropwise into the solution. After ten minutes, zinc precursor was then injected into the solution. This procedure was repeated twice to produce two monolayers of ZnS on the

nanoparticles. The reaction mixture was then cooled and transferred into the glovebox and divided evenly among two centrifuge tubes for extraction and cleaning. Methanol (30 ml) and hexanes (5 ml) were added to each mixture. Each solution was then was centrifuged at 9500 rpm for 5 minutes, with the supernatant retained. Hexanes (5 ml) and ethanol (30 ml) was added to the supernatant. The mixture was then centrifuged at 9500 rpm for 5 minutes, with the particles precipitating out of solution. The particles, a light brown powder, were then dried under vacuum and stored as a dry powder in a nitrogen filled glovebox.

2.3.2. Method 2: Using zinc oleate and thioacetamide.

Shelling was performed by modifying a procedure provided by Boercker *et al*.[67] A solution of zinc (0.02 M) was prepared by dissolving zinc oleate in 1-octadecene. The solution was degassed at 90°C, producing a clear, colorless solution, and cooled under N_2 to 50°C to prepare for injection. In a separate flask, a solution of thioacetamide in N,N-dimethylformamide (0.04 M) was prepared. In a separate flask, Zn_3P_2 nanoparticles (60 mg) in toluene (2 ml) were mixed with 1-octadecene (10 ml), trioctylphosphine oxide (0.33 g, 0.87 mmol), octadecylamine (1 g, 3.7 mmol), and trioctylphopshine (1.3 ml). The ligand solution was first degassed at 50°C prior to injection of the Zn_3P_2 core nanoparticles. The temperature was then raised to 80°C. At this time, the thioacetamide solution was injected dropwise into the solution. After ten minutes, zinc precursor was then injected into the solution. This procedure was repeated twice to produce two monolayers of ZnS on the nanoparticles. The reaction mixture was then cooled and transferred into the glovebox and divided evenly among two centrifuge tubes for extraction and cleaning. The core/shell nanoparticles were separated from unreacted precursors and byproducts by adding toluene (2 ml) and ethanol (15 ml) and centrifuging at 5000 rpm for 5 minutes. A dark brown precipitate formed at the bottom of the tubes after centrifuging, and the supernatants were discarded via decanting. The product was stored as a dispersion in toluene in a glovebox.

2.4. Characterization

Details of sample preparation, experimental conditions, and theoretical calculations can be found in the Supporting Information. XRD, bright field TEM, and HRTEM were used to identify the structure of our nanoparticles. STEM-EELS and XPS were used to perform elemental analysis for core/shell nanoparticles. Optical data was obtained from UV-VIS-NIR measurements and photoluminescence studies. Tauc plots were generated to extract optical band gaps.

3. Results and Discussion

X-ray diffraction confirmed our successful synthesis of α-Zn_3P_2 nanoparticles. As expected, we observed peak broadening from the nanostructuring of our materials; however, we observed an intense peak at 45 ° characteristic to the <400> plane of α-Zn_3P_2 (Figure 1).

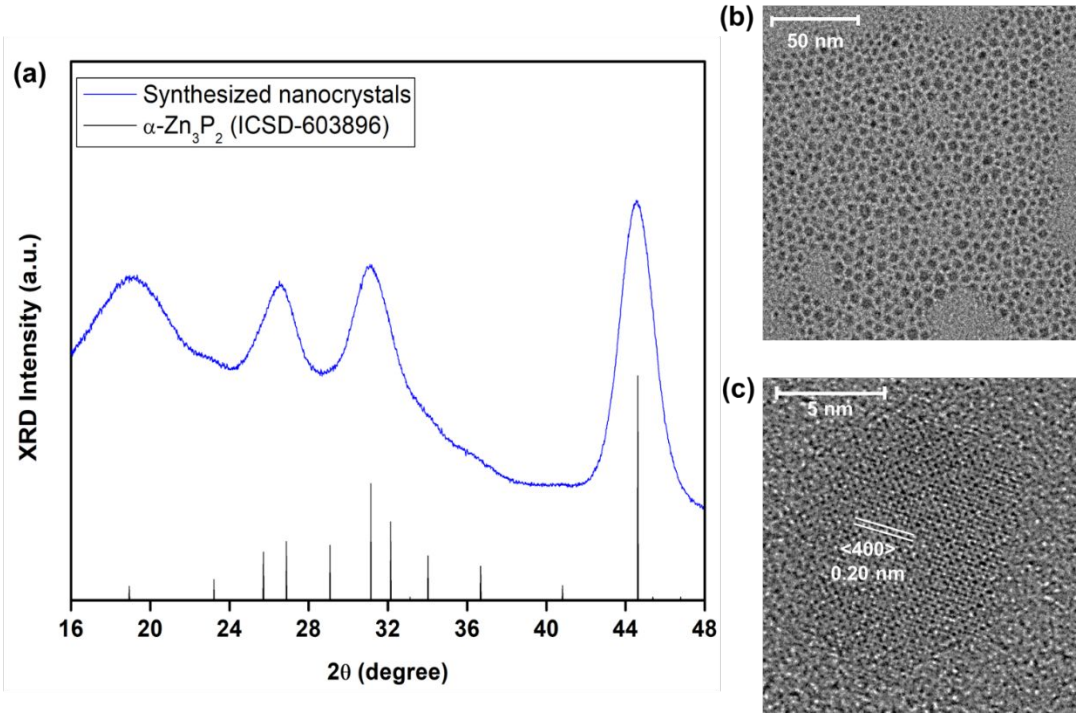

Figure 1. (a) Representative XRD pattern for synthesized α-Zn_3P_2 nanoparticles (reference: ICSD-603896). Nanoparticles were grown for 1 hour following injection of $P(SiMe_3)_3$ at 220°C. (b) Representative bright field image of synthesized nanoparticles. The average particle size was 3.5 ± 1.7 nm. (c) A HRTEM image of a synthesized nanoparticle. Calculation of d-spacing showed the characteristic <400> plane of α-Zn_3P_2.

In all instances, we observed partial surface oxidation of the nanoparticles via the formation of zinc phosphate tetrahydrate, as shown by the large, broadened peaks around 20° which might occur either during the synthesis, XRD data collection process, or a combination of both effects. Regardless, we were unable to prevent oxidation of these core-only nanoparticles. Changes in zinc precursor, time, concentration, and temperature had no influence on the crystal structure of our nanoparticles but affected the average particle size and size dispersity (Figures S1-S3). The average particle size ranged from 3.5 $\pm$ 1.7 nm to 5.7 $\pm$ 4.2 nm (Table 1). At diameters below 10 nm, the exciton Bohr radius of Zn_3P_2, we expected to observe quantum confinement (see Supporting Information for calculation). Control over the size dispersity of our batches was therefore important if these nanoparticles were to be used for optoelectronic applications. Note: we did not perform any size selective precipitation to obtain samples for transmission electron microscopy (TEM) imaging.

Table 1. Effect of Synthetic Conditions on Particle Size and Size Dispersity

Injection Temperature (°C)	Growth Temperature (°C)	Growth Time (h)	Amount of ODE (ml)	Mean Particle Size (nm)	Standard Deviation (nm)
160	220	2	30	4.1	1.4
180	220	2	30	3.9	1.2
200	220	2	30	4.0	1.1
220	220	2	30	5.4	4.2

220	220	1	30	3.5	1.7
220	220	4	30	4.0	1.6
220	220	2	15	Not successful	
220	220	2	60	4.5	1.2

To optimize our syntheses, we studied the effect of growth time, injection temperature, and concentration of precursors. We first studied the effect of growth time on the size and size distribution of our nanoparticles. Nanoparticles were grown for 1 to 4 hours at 220°C at an injection and growth temperature of 220°C. Nucleation and growth occurred rapidly; $P(SiMe_3)_3$, referred to as a "liquid source of PH_3," has been known to readily form metal phosphide compounds as it already contains phosphorus in a -3 oxidation state.[39] We therefore could not effectively control the size dispersity of our batches over time; between one and two hours of growth, the mean particle size increased from 3.5 nm ± 1.7 nm (Figure 2 a,b) to 5.4 ± 4.2 nm (Figure 2 c,d), but after four hours of growth, the mean particle size was 4.0 ± 1.1 nm (Figure 2 e,f). This size focusing effect may have occurred via digestive ripening.[68]

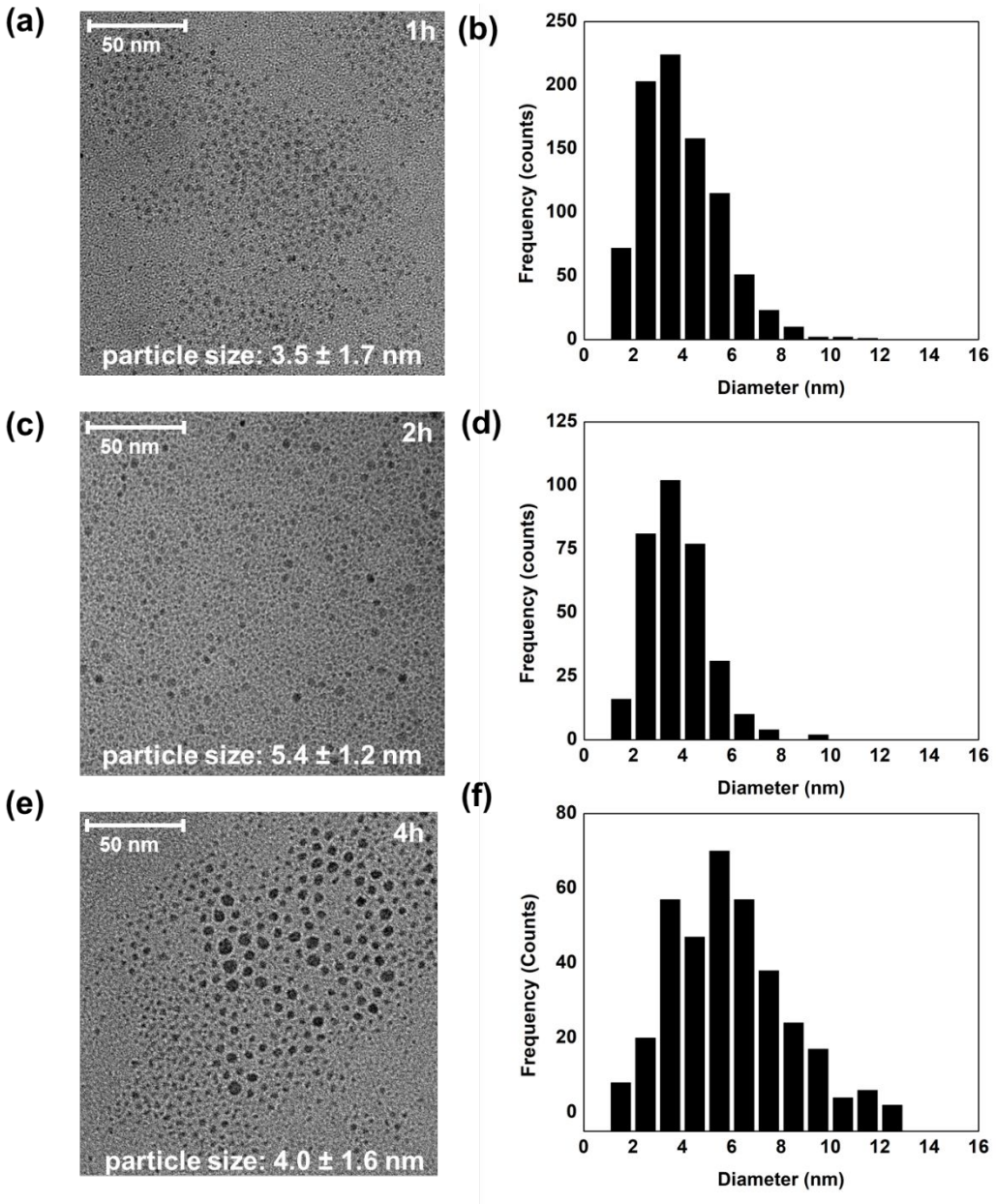

Figure 2. Bright field images and size distribution histograms for synthesized nanoparticles grown following injection of $P(SiMe_3)_3$ at 220°C for (a, b) 1 hour (c, d) 2 hours and (e, f) 4 hours. The mean particle size and standard deviation were obtained from a Gaussian distribution.

Owing to the fast reaction kinetics due to $P(SiMe_3)_3$, we decided to observe the effect of injection temperature on the growth mechanism of the nanoparticles as a control parameter. Since the particles were growing rapidly, we injected $P(SiMe_3)_3$ at a relatively low temperature to produce a small number of nuclei that would then rapidly grow as we increased the set temperature to the growth temperature of

220°C. We injected $P(SiMe_3)_3$ at 160°C, 180°C, 200°C, and 220°C. From 160 to 200°C, as the difference between the injection and growth temperature decreased, we obtained nearly the same average particle size of 4.0 nm (Figures 3 a, c, e), but the size distribution of the nanoparticles decreased from 1.4 nm to 1.1 nm (Figures 3 b, d, f). This size distribution was much smaller than the distribution obtained at a growth and injection temperature both of 220°C (5.4 ± 4.2 nm), confirming we could control reaction rate using the injection temperature.

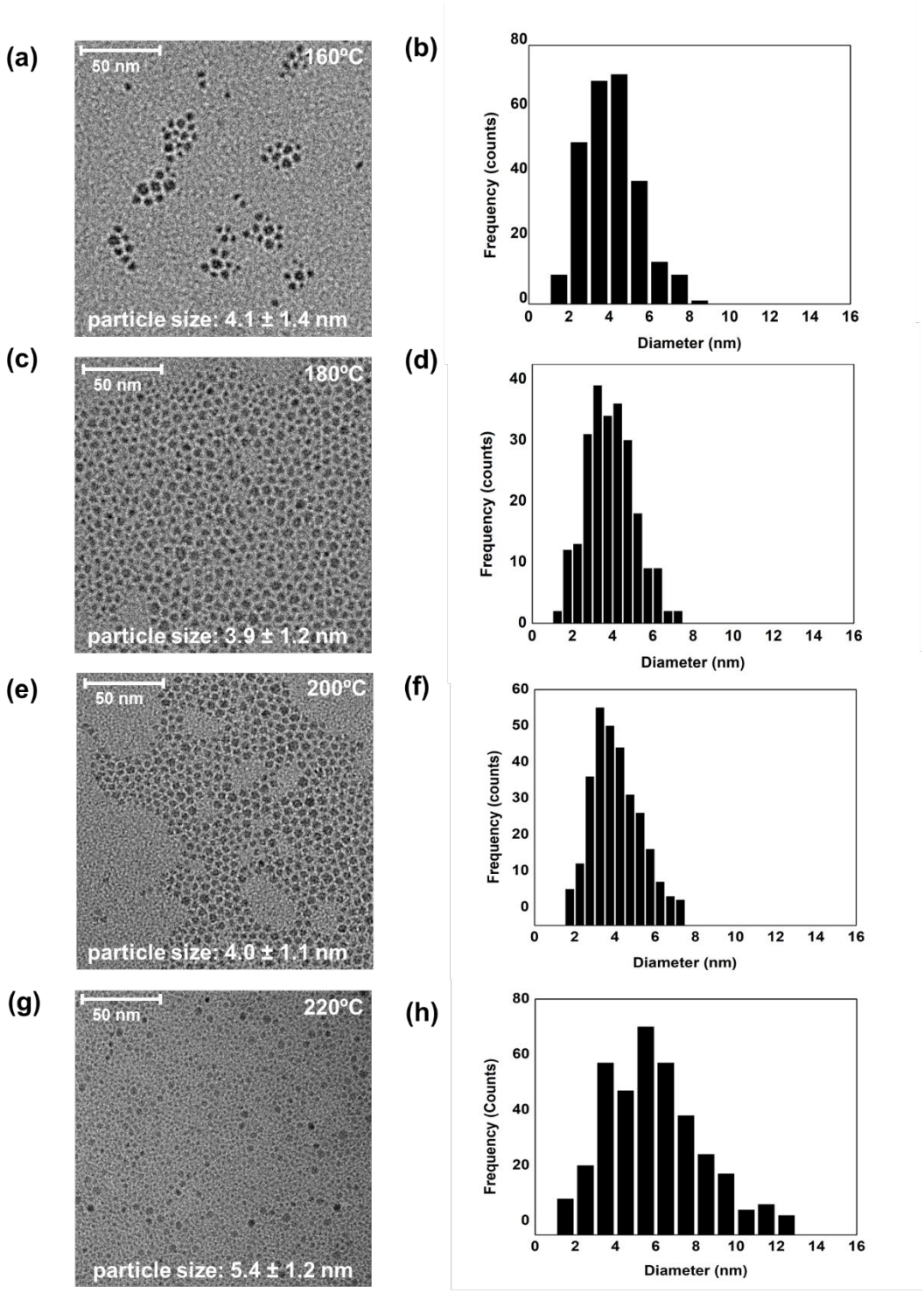

Figure 3. Bright field images and size distribution histograms for synthesized nanoparticles grown following injection of $P(SiMe_3)_3$ at (a, b) 160°C (c, d) 180°C (e, f) 200°C and (g, h) 220°C.

Finally, we varied the overall concentration of the precursors by changing the amount of the non-coordinating solvent systematically and performed experiments with 15 ml, 30 ml, and 60 ml of 1-octadecene. Nanoparticles were grown following injection of $P(SiMe_3)_3$ at 220°C for two hours. At 15 ml ODE, we found our particles were too small to be stable; we observed no zinc phosphide, only zinc phosphate and zinc hydroxide (Figure 4a). We hypothesize that at extremely high precursor concentrations (low volume of ODE), we generated a large number of nuclei and quickly exhausted all available precursors before the nuclei could grow to larger particles. Owing to their small size and large surface areas, these tiny nanocrystals quickly oxidized. At 30 ml and 60 ml ODE, however, we successfully synthesized Zn_3P_2 nanoparticles (Figures 4 b, c). From 30 ml to 60 ml, the mean particle size decreased from 5.4 ± 4.2 nm to 4.5 ± 1.2 nm. Typically, with decreasing precursor concentration, the rate of reaction decreases, producing fewer nuclei and therefore larger particles; if the reactions had gone to completion, the 60 ml reaction should have yielded the least number of nuclei and therefore the largest particles of the three concentrations tested. However, it seems that in our case, the 30 ml volume produced an intermediate number of nuclei, that at the faster reaction rate, produced larger particles in the set reaction time of two hours.

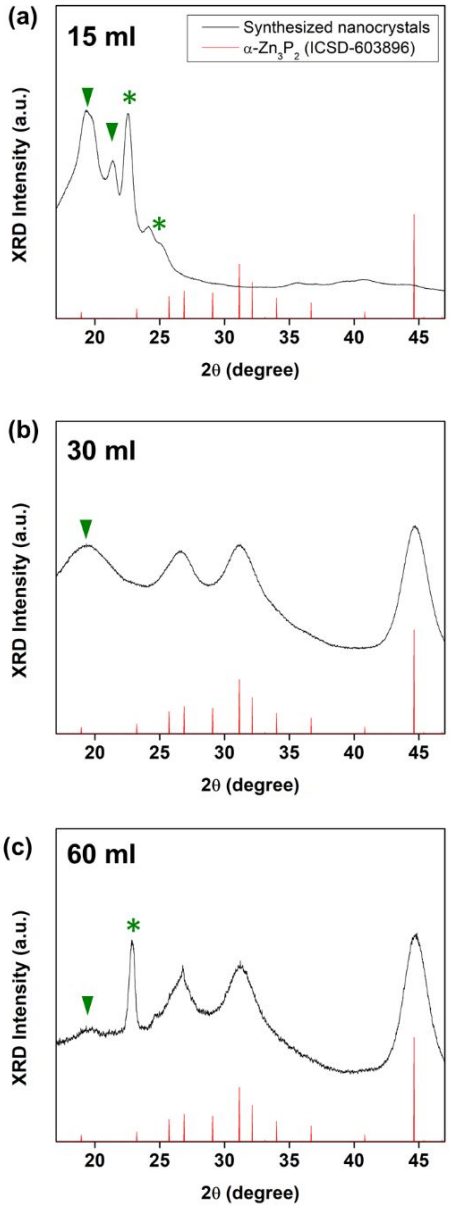

Figure 4. XRD patterns obtained for α-Zn_3P_2 nanoparticles (reference: ICSD-603896) grown for 2 hours following injection of $P(SiMe_3)_3$ at 220°C using (a) 15 ml (b) 30 ml and (c) 60 ml of ODE. At 15 ml ODE, we obtained small nanoparticles that oxidized quickly and completely to zinc phosphate tetrahydrate (reference: ICSD-34869, triangles) and zinc hydroxide (reference: ICSD-15008, asterisks). At 30 ml and 60 ml, we obtained zinc phosphide nanoparticles with signs of oxidation.

From these studies, we determined that the optimal synthesis conditions were injection of $P(SiMe_3)_3$ into the zinc carboxylate/ligand mixture at 200°C following growth at 220°C for 2 hours. Such syntheses resulted in the most monodisperse batches of those attempted. The absorption spectra of core nanocrystals

exhibited no sharp excitonic features regardless of synthesis conditions. We explored shelling of our nanoparticles with wide band gap ZnS to address these issues and improve the observed optical properties. To our knowledge, only Glassy *et al.* have reported an evident feature for 2.6 to 2.9 nm Zn_3P_2 nanocrystals with an unconfirmed crystal structure.[9, 32, 35, 41] Lack of an excitonic feature may be due to poor size dispersity; even after optimization of our synthesis, we observed size distribution from ± 26% to 78% for core nanocrystals. We did not observe any excitonic features regardless of size dispersity. Lack of an evident feature may also have been due to the presence of oxidation or silicon species in the nanocrystals from $P(SiMe_3)_3$ as observed by Miao *et al.*[41] They suspected that the silicon species, which may have a similar band gap to Zn_3P_2, acted as competitive low-lying traps for charge carriers.

Method 1: Using zinc acetate and elemental sulfur.

In the first method of overcoating, we activated elemental sulfur upon reaction with 1-octadecene at 190°C. Previous studies have shown that sulfur undergoes a polymerization reaction with alkenes at elevated temperatures. The products of these reactions are compounds with a polysulfur chain bonded to either the C_1 or C_2 position of the alkene.[69] In our procedure, we attempted to add two monolayers of ZnS on core Zn_3P_2 nanocrystals, under the assumption that each layer of ZnS adds 0.3 nm to the surface of the nanocrystal. For core nanoparticles 4.0 nm in size, we therefore expected to grow core/shell nanoparticles approximately 5.2 nm in diameter. However, our photoluminescence data suggested successful addition of one monolayer; we observed peak photoluminescence at 525 nm, indicating that we instead added one monolayer of ZnS to our nanocrystal (Figure 5).

In Miao *et al.*'s work, addition of a ZnO layer to the surface of Zn_3P_2 was thought to act as surface trapping sites for charge carriers, producing photoluminescence.[41] The addition of ZnS may have functioned similarly here for us. Still, after shelling, the absorption spectra exhibited no sharp excitonic features (Figure 6a).[9] The Tauc plots for core/shell nanocrystals estimated a direct band gap of approximately 2.75 eV (Figure 6b). Our results were consistent with predicted band gap calculations for

quantum confined particles of this size (see Supporting Information for calculation). However, bright field images of the core/shell nanoparticles showed that the nanoparticles exhibited poor colloidal stability, likely due to the presence of organosulfur compounds; previous studies have shown that S-ODE attaches to metal ions at the surface of nanocrystals, with organosulfur compounds present as ligands (Figure S4).[69] We also observed secondary nucleation and ZnS and ZnO (Figure S5). Secondary nucleation of ZnS was unsurprising as we aimed to grow a thick shell at an elevated temperature.[70] Despite these issues, we believe that the observed PL was obtained from some of the Zn_3P_2 nanocrystals that were successfully shelled; ZnO and ZnS are both wide band gap materials with band gaps of approximately 3.5 eV, corresponding to photoluminescence at approximately 350 nm and would not contribute to the observed photoluminescence at around 500 nm.[71-72]

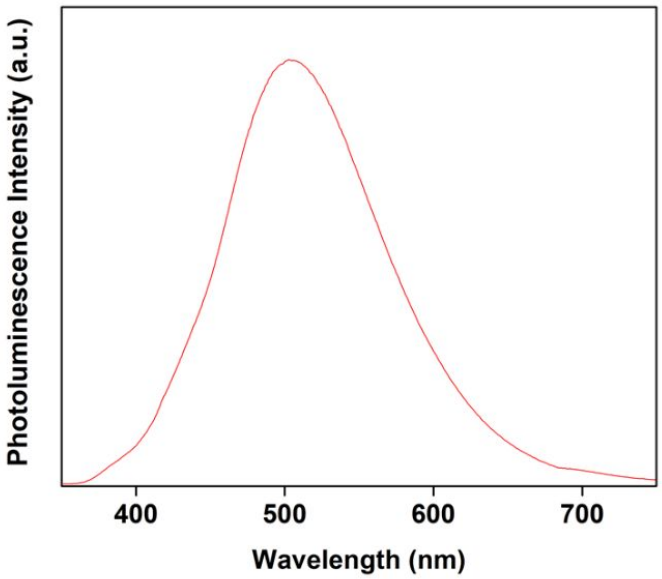

Figure 5. Photoluminescence of core/shell Zn_3P_2/ZnS nanoparticles. Samples were prepared in hexanes and read at an excitation wavelength of 300 nm. Peak emission occurred at 525 nm, consistent with the predicted band gap for Zn_3P_2 nanoparticles of this size.

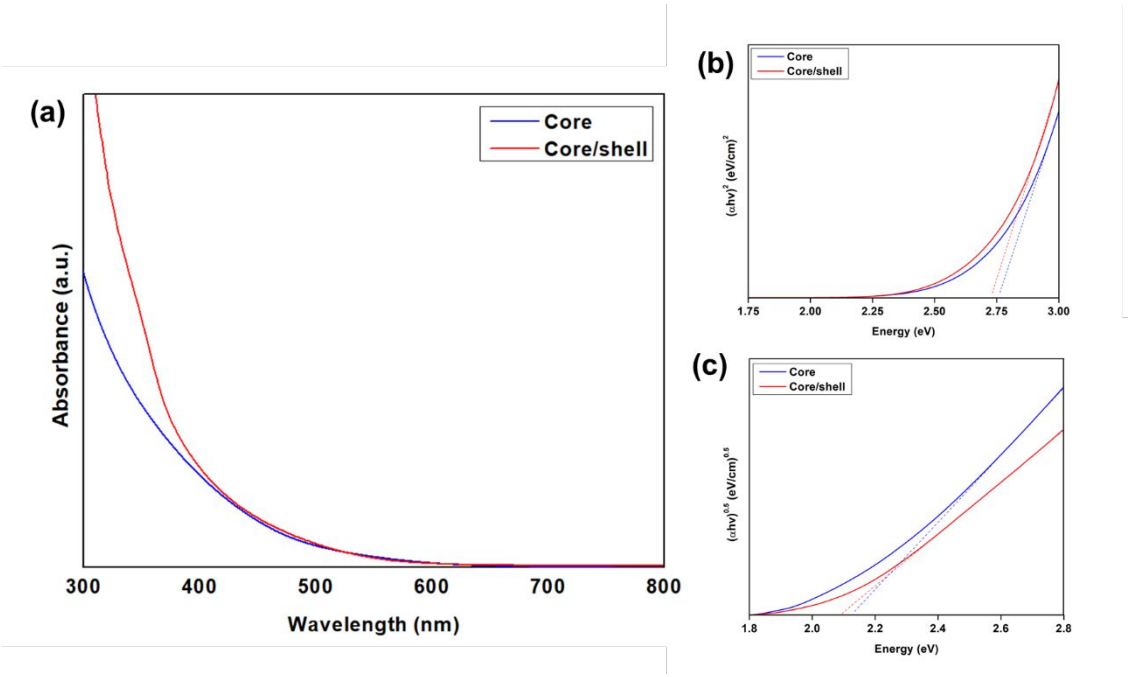

Figure 6. (a) Absorbance (a.u.) and corresponding (b) direct and (c) indirect Tauc plots for core (red) and core/shell (blue) nanoparticles for Method 1. Dotted lines show the estimated optical band gap extrapolated from the Tauc plots. The estimated direct band gap for core and core/shell nanocrystals was approximately 2.75 eV. The estimated indirect band gap was 2.1 eV.

Method 2: Using zinc oleate and thioacetamide

We performed two variations of Method 2. In the first variation, we dispersed Zn_3P_2 nanocrystals in a Zn oleate/ODE solution and added thioacetamide dropwise to the mixture. We observed photoluminescence at 480 nm with an excitation wavelength of 380 nm. PLE data obtained with an emission of 480 nm corroborated that photoluminescence came from the nanocrystals (Figure 7). We did not observe sharp excitonic features (Figure 8a). The calculated Tauc plot data estimated that the optical band gap was approximately 2.6 eV (Figure 8b). These results suggested that we synthesized core/shell nanocrystals of approximately 4 nm in diameter; this was unexpected as core Zn_3P_2 nanocrystals were 4.0 ± 1.1 nm in size. However, we believe this was possible according to the reaction mechanism proposed by Boercker *et al*. for shelling of PbS nanocrystals stabilized by carboxylate ligands.[67] In their work, Boercker *et al.* suggested that addition of thioacetamide removes original carboxylate ligands on the surface of the nanocrystal to react with Pb. Zinc oleate then reacts to the surface, adding back oleate ligands to passivate

the nanocrystal. As we performed our reactions in a similar chemical environment, we suspect that thioacetamide similarly stripped carboxylate ligands from the surface of Zn_3P_2 nanocrystals to add sulfur to the surface. Stripping may have caused dissolution of some surface Zn, so that the Zn_3P_2 core was smaller than 4.0 nm and shell addition did not lead to an apparent increase in particle size.

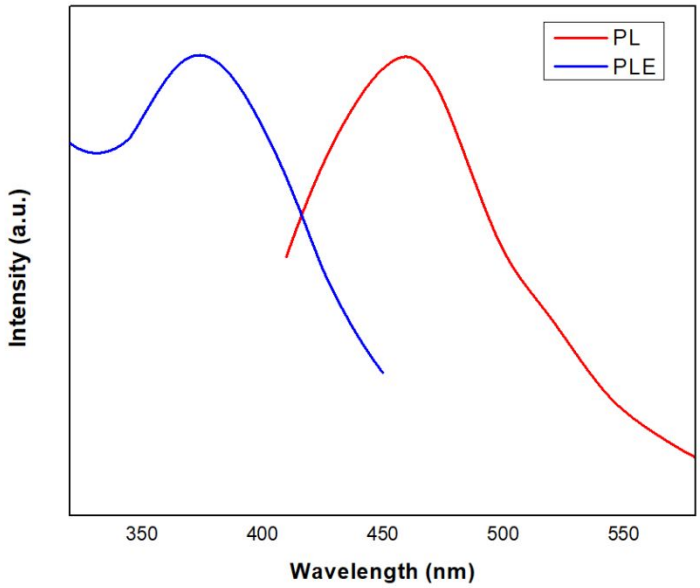

Figure 7. Photoluminescence excitation (PLE, blue) and photoluminescence (PL, red) spectra for core/shell nanocrystals with an estimated two monolayers of ZnS added to the core nanocrystals, following the protocol from Boercker *et al.*[67]

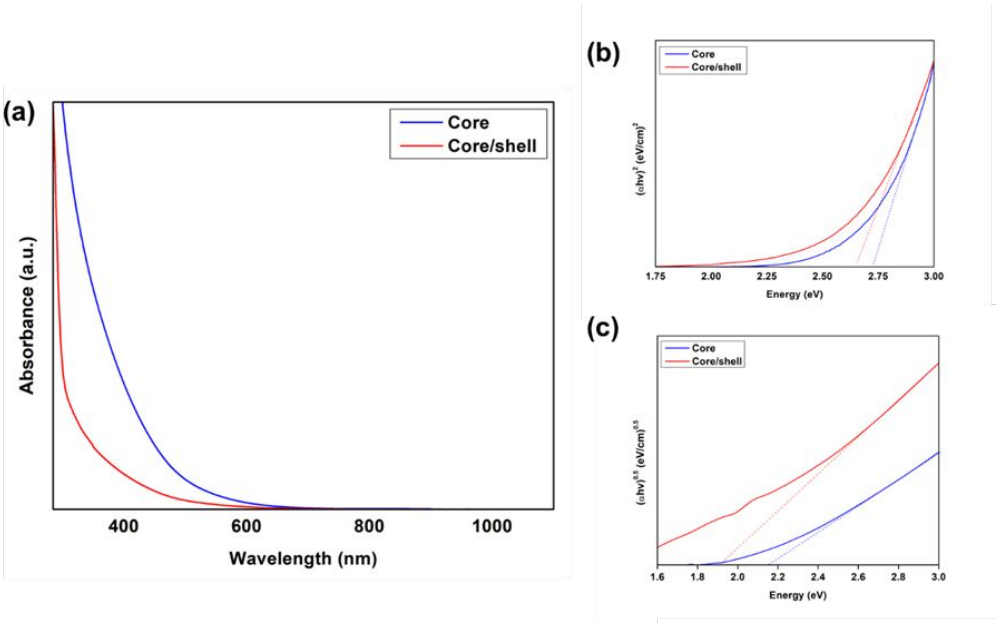

Figure 8. (a) Absorbance (a.u.) and corresponding (b) direct and (c) indirect Tauc plots for core (blue) and core/shell (red) nanoparticles for Method 2. Dotted lines show the estimated optical band gap extrapolated from the Tauc plots. The estimated direct band gap was 2.75 eV for core Zn3P2 nanocrystals and 2.6 eV for core/shell Zn3P2/ZnS nanoparticles. The estimated indirect band gap was 2.2 eV for core nanocrystals and 1.9 eV for core/shell nanocrystals.

We grew a full shell of ZnS by modifying the procedure to incorporate more stabilizing ligands (TOPO, ODA, and TOP) into the solution. From bright field TEM images, we observed the mean particle size increased from 4.0 ± 1.1 nm for core nanoparticles to 4.7 nm ± 1.0 nm for core/shell nanoparticles (Figure 9a). Scanning TEM (STEM)–electron energy loss spectroscopy (EELS) elemental maps (Figure 9b-d) confirmed the presence of sulfur on the surface predominantly, thus proving successful growth of the ZnS shell. PXRD also suggested a thick shell growth (Figure 5); from our calculations (detailed in the Supporting Information), we predicted the addition of two monolayers of ZnS to our particles. From the increase in observed size of the particles, nearly one monolayer (~0.35 nm) of ZnS is possibly added but there also might be slight alloying at the interface which might increase the ZnS content. Additional images can be found in the supplementary information (Figure S6). XPS data taken at the sulfur edge

also confirmed the presence of sulfur via the appearance of an S($2p_{3/2}$) peak in Zn_3P_2/ZnS nanoparticles at 162 eV (Figure S7). The peak position was typical for that for zinc sulfide.[73]

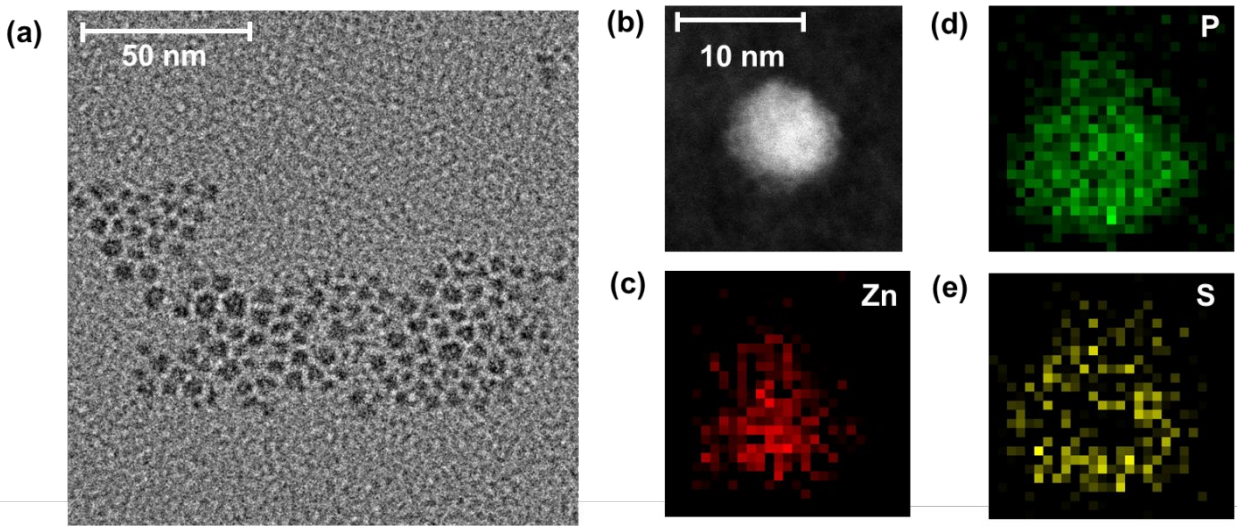

Figure 9. (a) A bright field TEM image of core/shell Zn_3P_2/ZnS nanoparticles, with a mean particle size of 4.7 nm ± 1.0 nm. (b-e) High angle annular dark field-STEM image and (c-e) STEM-EELS elemental maps of a single Zn_3P_2/ZnS core/shell nanocrystal confirmed the presence of sulfur.

The core/shell particles were also more stable, lasting against oxidation outside of the glovebox in ambient conditions (Figure S8). Miao *et al*., who synthesized Zn_3P_2 from zinc stearate and $P(SiMe_3)_3$, suggested the poor optical properties was due to the use of $P(SiMe_3)_3$.[41] They attributed the lack of photoluminescence to the incorporation of silicon species into the crystal lattice generated from tris(trimethylsilyl)phosphine, which they confirmed was present via TEM-EDS. They suspected that the silicon species, which may have a similar band gap to Zn_3P_2, acted as competitive low-lying traps for charge carriers that decrease PL efficiency. Addition of the ZnO layer to the surface of Zn_3P_2 was thought to act as surface trapping sites for charge carriers, producing photoluminescence. The addition of ZnS may have functioned similarly here for us; upon shelling, we observed photoluminescence with a peak at 520 nm which we attribute to band edge recombination (Figure 10). Studies also showed a second peak of much lower intensity at 700 nm. which might be due to trap state emission. Previous studies on

nanoscale Zn_3P_2/ZnS nanoribbon/nanowire heterostructures claimed that emission in this range could come from surface sulfur species present in ZnS, while the lower energy emission arises from band edge emission of Zn_3P_2.[66] In our case, however, we did not observe any ZnS impurities in TEM and as defect states for non-quantum confined Zn_3P_2 should appear at energies lower than 1.5 eV, we attribute the photoluminescence to quantum confinement of Zn_3P_2, with ZnS acting as a passivating layer in a type I heterostructure. This conclusion is consistent with the predicted optical band gap of between 2.0 to 2.5 eV for quantum confined particles 4 nm to 5 nm in size (Table S1). Peak luminescence at this wavelength was also consistent with the estimated optical band gap of 2.5 eV from the Tauc plot of core Zn_3P_2 nanoparticles. Previous studies on Zn_3P_2/ZnS heterostructures have predicted type II behavior, though type I behavior as shown here has also been observed.[27, 50, 65, 74-75]

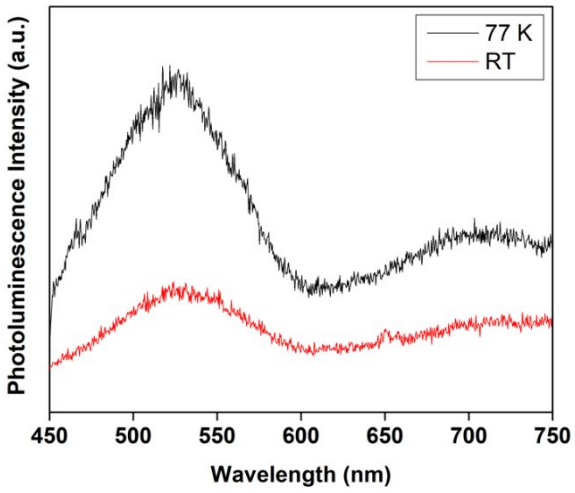

Figure 10. Photoluminescence data of Zn_3P_2/ZnS thin films at 77 K (black) and room 7 temperature (red). The excitation wavelength for these studies was 400 nm. Samples were dropcasted from a dispersion in toluene. Measurements show peak emission at 525 nm and 700 nm.

We are currently conducting further studies to understand the nature of the trap sites and observed photoluminescence in this material. Initial time resolved studies estimated average lifetimes of around 0.18 ± 0.15 ns at RT and 0.18 ± 0.08 ns at 77 K from a biexponential fit (Figure S9-S10). Others

previously reported lifetimes for Zn_3P_2 and Zn_3P_2/ZnO. For bulk Zn_3P_2, Kimball *et al.* reported carrier lifetimes of $\tau_1 = 4$ ns and $\tau_2 = 20$ ns from a biexponential fit, or an average lifetime of 18 ns.[27] H*o et al.* reported τ_1 = 2.96 ± 013 ns to 0.60 ± 002 ns and τ_2 = 20.76 ± 7.01 ns to 4.66 ± 0.42 ns for 4.8 ± 0.7 nm to 8.8 ± 0.13 nm Zn_3P_2 nanocrystals.[35] For Zn_3P_2/ZnO core/shell nanocrystals, Miao *et al.* reported much longer lifetimes of 216 to 423 ns from biexponential fits, indicating emission likely due to defect states rather than band edge emission.[41] To the best of our knowledge, our work is the first report of lifetime measurements for the Zn_3P_2/ZnS system.

The exact nature of our peak and its contribution to the optical properties of the quantum dots is currently under investigation. In our biexponential fit, τ_1 = 0.07 ns for τ_2 = 0.4 ns at RT (Table S1). The difference in the two decay times suggested that they arose from excited states of different natures. The fast PL decay component, τ_1, may have originated from the recombination of delocalized carriers in the internal states within the nanocrystal representing the lifetime of the band-edge emission decay; the slow PL decay component, τ_2, can be assigned to the recombination of the localized carriers at the surface, where both radiative and non-radiative traps can exist. However, the relatively fast lifetimes and the tiny difference between them at RT and 77 K indicated that the emission has a nearly single-exponential decay, thus suggesting weak contribution of defects in the electron/hole recombination process. This hypothesis was strengthened by the fact that the PL was observed only post-shelling wherein the surface recombination traps were most likely passivated by the ZnS shell. Additionally, at 77 K, the decay process was essentially single-exponential with a fast lifetime of ~0.2 ns, suggesting band edge recombination following fast intra-band relaxation due to efficient electron–phonon/hole coupling.

4. Conclusions

In this work, we synthesized crystalline α-Zn_3P_2 nanoparticles from zinc carboxylates and $P(SiMe_3)_3$. We controlled the average particle size and size dispersity of our batches via the injection temperature of

$P(SiMe_3)_3$. In the optimal synthesis, we obtained 4.0 ± 1.1 nm sized particles. The core Zn_3P_2 nanoparticles themselves exhibited no luminescence or distinct excitonic features, likely due to surface oxidation and presence of impurities from $P(SiMe_3)_3$ in the crystal structure. Post-synthetic addition of a ZnS shell provided measurable photoluminescence at 520 nm from 4.7 ± 1.0 nm particles with short lifetimes of 0.18 ns. Future study will focus on understanding the origin of the observed optical properties.

Supporting Information

Supporting Information is available from *Nanoscale* or from the author.

Acknowledgements

IJP acknowledges support by the U.S. Department of Energy, Office of Science, Office of Workforce Development for Teachers and Scientists, Office of Science Graduate Student Research (SCGSR) program. The SCGSR program is administered by the Oak Ridge Institute for Science and Education (ORISE) for the DOE. ORISE is managed by ORAU under contract number DE-SC0014664. All opinions expressed in this paper are the author's and do not necessarily reflect the policies and views of DOE, ORAU, or ORISE. This research used resources of the Center for Functional Nanomaterials, which is a U.S. DOE Office of Science Facility, at Brookhaven National Laboratory under Contract No. DE-SC0012704. Z. Lian acknowledges support from NYSTAR through Focus Center-NY–RPI Contract C150117. S.-F. Shi acknowledges support from AFOSR through Grant FA9550-18-1-0312. We are grateful for the assistance of Tony Hu at the Department of Chemistry of New York University with the X-ray analysis, and we thank the support to the X-ray facility by the National Science Foundation under Award Numbers CRIF/CHE-0840277 and by the NSF MRSEC Program under Award Number DMR-0820341 and DMR-1420073. Tai-De Li, Sheng Zheng, and Tong Wang of the Imaging and 26Surface Science Facilities of CUNY Advanced Science Research Center instrument use, scientific and technical assistance.

Conflict of Interest

The authors report no conflict of interest.

Author Contributions

K. M. M. and A. S. conceived the project. A. S. supervised the project. C. B. and A.S. performed all preliminary syntheses and characterization. I. J. P., S. Lee, and S. C. optimize synthesis for core-only and core/shell nanocrystals. I. J. P. and S. Lee prepared thin films for and performed XRD measurements. I. J. P. performed LRTEM and HRTEM imaging and solution-based optical measurements. M. K. and M. R. S. prepared thin films for and performed XPS measurements. S. Li and S. H. performed STEM imaging and elemental analysis. Z. L. and S. S. performed photoluminescence measurements on thin films. I. J. P. and A. S. analyzed the data. All authors contributed to preparation of the manuscript.

References

[1] P. Reiss, M. Carrière, C. Lincheneau, L. Vaure, and S. Tamang, *Chem. Rev.* **2016**, *116* (18), 10731.

[2] H. Li, C. Jia, X. Meng, and H. Li, *Front. Chem.* **2019***, 6*, 652.

[3] S. Carenco, D. Portehault, C. Boissière, N. Mézailles, and C. Sanchez, *Chem. Rev.* **2013** *113* (10), 7981.

[4] Y.-H. Won, O. Cho, T. Kim, D.-Y. Chung, T. Kim, H. Chung, H. Jang, J. Lee, D. Kim, and E. Jang, *Nature* **2019** 575, 634.

[5] C. Candelise, M. Winskel, and R. Gross, *Prog. Photovoltaics* **2012,** *20* (6), 816.

[6] A. K. Jena, A. Kulkarni, and T. Miyasaka, *Chem. Rev.* **2019**, *119* (5), 3036.

[7] NREL, Best Research-Cell Efficiency Chart, https://www.nrel.gov/pv/cell-efficiency.html accessed: February, **2020**.

[8] K. Rudisch, Y. Ren, C. Platzer-Björkman, and J. Scragg, *Appl. Phys. Lett.* **2016,** *108* (23), 231902.

[9] B. A. Glassy and B. M. Cossairt, *Small* **2017**, 13, 1702038.

[10] C. Wadia, A. P. Alivisatos, and D. M. Kammen, *Environ. Sci. Technol.* **2009,** *43* (6), 2072.

[11] V. S.Vavilov, V. D. Negrei, I. V. Potykevich, Y. V. Potykevich, A. V. Fedotovskii, and M. V. Chukichev, *Phys. Status Solidi B* **1972,** *49* (1), K103.

[12] I. S. Gorban, V. V.Lugovskii, A. P. Makovetskaya, I. I. Tychina, and A. V. Fedotovskii, *Sov. Phys. Semiconductors* **1974,** *8* (2), 283.

[13] V. V. Sobolev, A. I. Kozlov, and S. G. Kozlova, *Opt. Spectrosc.* **1994**, 77(5), 706.

[14] V. V. Sobolev and A. I. Kozlov, *Phys. Status Solidi B* **1984,** *126* (1), K59.

[15] V. V. Sobolev and N. N. Syrbu, *Phys. Status Solidi B* **1974,** *64* (2), 423.

[16] A. E. Fagen, Optical properties of Zn_3P_2. *J. Appl. Phys.* **1979,** *50* (10), 6505.

[17] M. P. Lisitsa, P. E. Mozol, I. I. Tychina, I. V. Fekeshgazi, and A. V. Fedotovskii, *Quantum Electron.* **1975,** *4* (9), 1159.

[18] M. P. Lisitsa, P. E. Mozol, I. I. Tychina, I. V. Fekeshgazi, and A. V. Fedotovskii, *Quantum Electron.* **1975,** *4* (9), 1.

[19] N. C. Wyeth and A. Catalano, *J. Appl. Phys*. **1980,** *51* (4), 228.

[20] N. C. Wyeth and A. Catalano, *J. Appl. Phys*. **1979,** *50* (2), 1403.

[21] P. S. Nayar and A. Catalano, *Phys. Lett.* **1981,** *39* (1), 105.

[22] A. Catalano and M. Bhushan, *Appl. Phys. Lett.* **1980,** *37* (6), 567.

[23] A. Catalano and R. B. Hall, *J. Phys. Chem. Solids* **1980,** *41* (6), 635.

[24] M. Bhushan and A Catalano, *Appl. Phys. Lett.* **1981,** *38* (1), 39.

[25] K. Shportko, T. Barlas, and E. Venger, H. El-Nasser, *Curr. Appl. Phys.* **2016,** *16*, 8.

[26] J. Collier and S. Wu, D. Apul, *Energy* **2014,** *74*, 314.

[27] G. M. Kimball, A. M. Müller, N. S. Lewis and A.H. Atwater, *Appl. Phys. Lett.* **2009,** *95* (11), 112103.

[28] G. M. Kimball, N. S. Lewis, and A. H. Atwater, Mg doping and alloying in Zn_3P_2 heterojunction solar cells. Presented at 2010 35th IEEE Photovoltaic Specialists Conference, Honolulu, HI, **2010**.

[29] A. M. Hermann, A. Madan, M. W. Wanlass, V. Badri, R. Ahrenkiel, S. Morrison, and S. C. Gonzalez, *Sol. Energy Mater. Sol. Cells* **2004,** *82* (1), 24.

[30] O. Vazquez-Mena, J. P. Bosco, O. Ergen, H. I. Rasool, A. Fathalizadeh, M. Tosun, M. Crommie, A. Javey, H. A. Atwater, and A. Zettl, *Nano Lett.* **2014,** *14* (8), 4280.

[31] H. Weller, A. Fojtik, and A. Henglein, *Chem. Phys. Lett.* **1985,** *117* (5), 485.

[32] B. A. Glassy and B. M. Cossairt, *Chem. Comm.* **2015,** *51* (25), 5283.

[33] B. A. Glassy and B. M. Cossairt, *Chem. Mater.* **2016,** *28* (17), 6374.

[34] S. Carenco, M Demange, J. Shi, C. Boissiere, C. Sanchez, P. Le Floch and N. Mezailles, *Chem. Comm.* **2010,** *46* (30), 5578.

[35] M. Q. Ho, J. A. Esteves, G. Kedarnath, and I. U. Arachchige, *J. Phys. Chem. C.* **2015,** *119* (19), 10576.

[36] T. H. Lim, G. T. Be, and R. D. Tilley, *Key Eng.* **2016,** *701*, 3.

[37] M. Green and P. O'Brien, *Chem. Mater.* **2001,** *13* (12), 4500.

[38] E. J. Luber, M. H. Mobarok and J. M. Buriak, *ACS Nano.* **2013**, *7* (9), 8136.

[39] M. H. Mobarok, E. J. Luber, G. M. Bernard, L. Peng, R. E. Wasylishen and J. M. Buriak, *Chem. Mater.* **2014**, *26* (5), 1925.

[40] M. H. Mobarok and J. M. Buriak, *Chem. Mater.* **2014**, *26* (15), 4653.

[41] S. Miao, T. Yang, S. G. Hickey, V. Lesnyak, B. Rellinghaus, J. Xu and A. Eychmüller, *Small* **2013**, *9* (20), 3415.

[42] M. E. Mundy, D. Ung, N. L. Lai, E. P. Jahrman, G. T. Seidler and B. M. Cossairt, *Chem. Mater.* **2018**, *30* (15), 5373.

[43] K. Lee, Y. Huang and J. F. Corrigan. *Chem. Comm.* **2019**, *55* (76), 11466.

[44] G. Shen, C. Ye, D. Golberg, J. Hu and Y. Bando, *Appl. Phys. Lett.* **2007**, *90* (7), 073115.

[45] G. Shen, G.; P. C. Chen, Y. Bando, D. Golberg and C. Zhou, *J. Phys. Chem. C* **2008**, *112* (42), 16405.

[46] C. Liu, L. Dai, L. P. You, W. J. Xu, R. M. Ma, W. Q. Yang, Y. F. Zhang, and G. G. Qin, *J. Mater. Chem*. **2008**, *18* (33), 3912.

[47] P. Wu, T. Sun, Y. Dai, Y. Sun, Y. Ye, and L. Dai, *Cryst. Growth Des.* **2011**, *11* (5), 1417.

[48] P. Wu, Y. Dai, Y. Ye, Y. Yin, and L. Dai, *Journ. of Mater. Chem.* **2011**, *21* (8), 2563.

[49] I. T. Bae, P. Vasekar, D. VanHart, and T. Dhakal, *Mater. Res.* **2011**, *26* (12), 1464.

[50] T. Sun, P. C. Wu, Z. D. Guo, Y. Dai, H. Meng, X. L. Fang, Z. J. Shi, L. Dai and G. G. Qin, *Phys. Lett. A.* **2011**, *375* (21), 2118.

[51] B. Lance, V. Venkata and V. Sreeram, *Nanotechnology.* **2014**, *25* (12), 125402.

[52] B. Lance, V. Venkata, A. A. Hasti, S. Y. Reza and V. Sreeram, *Nanotechnology.* **2014**, *25* (14), 145401.

[53] J. Y. Chen, L. C. Chin, G. A. Li and H. Y. Tuan,. *Cryst. Eng. Comm.* **2017**, 19, 975.

[54] X. Li, W. Li, J. Yu, H. Zhang, Z. Shi and Z. Guo,. *J. Alloys Compd.* **2017**, *724*, 932.

[55] Y. Chen, R. Polinnaya and S. Vaddiraju, *Mater. Res. Express* **2018**, *5* (5), 055042.

[56] L. Brockway, M. Van Laer, Y. Kang and S. Vaddiraju, *Phys. Chem. Chem. Phys.* **2013**, *15* (17), 6260.

[57] G. Shen, Y. Bando and D. Golberg, *J. Phys. Chem. C* **2007**, *111* (13), 5044.

[58] G. Shen, P. Chen, Y. Bando and D. Golberg, C. Zhou, *Chem. Mater.* **2008**, *20* (23), 7319.

[59] G. Shen, Y. Bando, Y.; J. Q. Hu and D. Golberg, *Appl. Phys. Lett.* **2006**, *88* (14), 143105.

[60] R. A. Swain, B. McVey, H. Virieux, F. Ferrari, Y. Tison, H. Martinez, B. Chaudret, C. Nayral and F. Delpech, *Chem. Comm.* **2020**.

[61] D. Chen, A. Wang and M. A. Buntine, *Chem. Electro. Chem.* **2019**, *6* (18), 4709.

[62] N. Y. Dzade, *Phys. Chem. Chem. Phys*. **2020**, *22* (3), 1444.

[63] H. Zhu, A. Prakash, D. N. Benoit, C. J. Jones and V. L. Colvin, *Nanotechnology* **2010**, *21* (25), 255604.

[64] P. Reiss and M. Protière, L. Li, *Small* **2009**, *5* (2), 154.

[65] J. P. Bosco, S B. Demers, G. M. Kimball, N. S. Lewis and H. A. Atwater, *J. Appl. Phys.* **2012**, *112* (9), 093703.

[66] D. Chen, Z. Liu, X. Wang, B. Liang, J. Xu, H. Huang, Z. Xie and G. Shen, *Cryst. Eng. Comm.* **2011**, *13* (24), 7305.

[67] J. E. Boercker, D. L. Woodall, P.D. Cunningham, D. Placencia, C. T. Ellis, M. H. Stewart, T. H. Brintlinger, R. M. Stroud and J. G. Tischler, *Chem. Mater.* **2018**, *30* (12), 4112.

[68] J. R. Shimpi, D.S. Sidhaye and B. L. V. Prasad, *Langmuir*, **2017**, *33* (38), 9491.

[69] M. R. McPhail and E. A. Weiss., *Chem. Mater.* **2014**, 26 (11), 3377-3384.

[70] J. Park, A. Jayaraman, X. Wang, J. Zhao, and H.-S. Han, *ACS Nano* **2020**.

[71] K.-F. Lin, H.-M. Cheng, H.-C. Hsu, L.-J. Lin, and W.-F. Hsieh, *Chem. Phys. Lett.* **2005**, *409* (4), 208-211.

[72] I. L. Medintz, H. T. Uyeda, E. R. Goldman, and H. Mattoussi, *Nat. Mater.* **2005,** *4* (6), 435-446.

[73] A. V. Naumkin, S. W. Gaarenstroom and C. J. Powell, NIST x-ray photoelectron spectroscopy database, 2012. https://srdata.nist.gov/xps/main_search_menu.aspx accessed: December, **2019**.

[74] M. Kaur, K. Kabra, R. Kumar, B. K. Sharma and G. Sharma, *J. Electron. Mater.* **2016,** *45* (6), 2847.

[75] I. G. Stamov, N. N. Syrbu and A. V. Dorogan, *Physica B Condens. Matter.* **2013,** *408*, 29.